How to cite: *Angew. Chem. Int. Ed.* **2025**, e17603
doi.org/10.1002/anie.202517603

Supramolecular Chemistry **Very Important Paper**

Thermally Activated Stereoinversion in Benzotrithiophene-Based Supramolecular Polymers with Water as the Effector

Lucía López-Gandul[+], Alberto Fernández-Alarcón[+], Nicolás M. Casellas, Cristina Naranjo, Joaquín Calbo, Enrique Ortí,* Miguel García-Iglesias,* and Luis Sánchez**

Abstract: We report the synthesis of the chiral benzotrithiophene (BTT) derivative **1**, which self-assembles into helical supramolecular polymers. The C_3 symmetry of BTT **1** enables a unique temperature-dependent stereomutation process in which water acts as a key effector. Circular dichroism measurements reveal that a higher water content induces a double stereomutation, ultimately restoring the original helicity. In contrast, reducing the water content leads to a single, stable stereomutation, which duration depends on the amount of water in solution. To elucidate the stereomutation mechanism, we conducted a multi-level computational study, identifying two main conformations for the monomeric species that lead to diastereomeric helices with different preferred handedness, thus resulting in opposite dichroic patterns. The transition between these aggregates involves rotation of the BTT cores and amide groups, a process significantly facilitated by water molecules via triple hydrogen bonding within the helical stack. These findings exhibit the crucial role of the solvent in modulating chiral supramolecular polymer structures and provide unprecedented insights into the influence of water on self-assembly and stereomutation processes.

Introduction

Solvent–solute interactions play a crucial role in life sciences, influencing solubility, reactivity, and, especially, molecular organization. They determine how molecules dissolve and behave in solution, affecting reaction outcomes and material properties.[1] Among the large variety of solvents, water is crucial to favor the self-assembly of biomolecules that eventually generate complex systems exhibiting adaptability and robustness.[2] Polypeptides and polynucleotides exemplify the role of these water-solute interactions in stabilizing the tertiary structure of such natural polymers, where noncovalent forces play a pivotal role.[3,4] Beyond biological systems, solvent–solute interactions also influence the self-assembly and disassembly of synthetic scaffolds capable of forming supramolecular polymers, in which the monomeric units are bonded by noncovalent forces.[5] In supramolecular polymers, the solvent–solute interactions are as strong as those maintaining the polymeric structure and dictate the final outcome of the supramolecular polymerization process.[6–9]

Despite the number of supramolecular ensembles attained by self-assembly of amphiphilic systems in water,[10–12] the supramolecular polymerization of organic scaffolds is usually studied in nonpolar alkanes as solvents.[6–9] These nonpolar solvents optimize the operation of noncovalent forces like H-bonding and π-stacking interactions during the self-assembling process.[13] However, they contain low, but still relevant, amounts of water. These water molecules possess potential enthalpic energy, stemming from the unrealized hydrogen bonds, and can strongly condition the self-assembling features of a variety of systems. Their interaction with the target structures can give rise to competitive pathways, leading to different helical aggregated species.[14]

Formally, competitive pathways constitute a relevant example of stereomutation in supramolecular polymers, in which a single enantioenriched monomeric species can generate aggregated species of opposite helicity. Stereomutation, as a manifestation of dynamic stereochemistry,[15–17] has been observed both in molecular[18] and supramolecular[19–21] species. Supramolecular stereomutation is of particular interest due to its potential for constructing chiroptical

[*] Dr. L. López-Gandul[+], Dr. C. Naranjo, Prof. Dr. L. Sánchez
Departamento de Química Orgánica, Facultad de Ciencias Químicas, Universidad Complutense de Madrid, Ciudad Universitaria s/n, Madrid 28040, Spain
E-mail: lusamar@ucm.es

Dr. A. Fernández-Alarcón[+], Dr. J. Calbo, Prof. Dr. E. Ortí
Instituto de Ciencia Molecular (ICMol), Universidad de Valencia, c/ Catedrático José Beltrán 2, Paterna, Valencia 46980, Spain
E-mail: joaquin.calbo@uv.es
enrique.orti@uv.es

Dr. N. M. Casellas, Dr. M. García-Iglesias
QUIPRE Department, Nanomedicine-IDIVAL, Universidad de Cantabria, Avd. de Los Castros 46, Santander 39005, Spain
E-mail: giglesiasm@unican.es

[+] Both authors contribute equally to this work.

Additional supporting information can be found online in the Supporting Information section

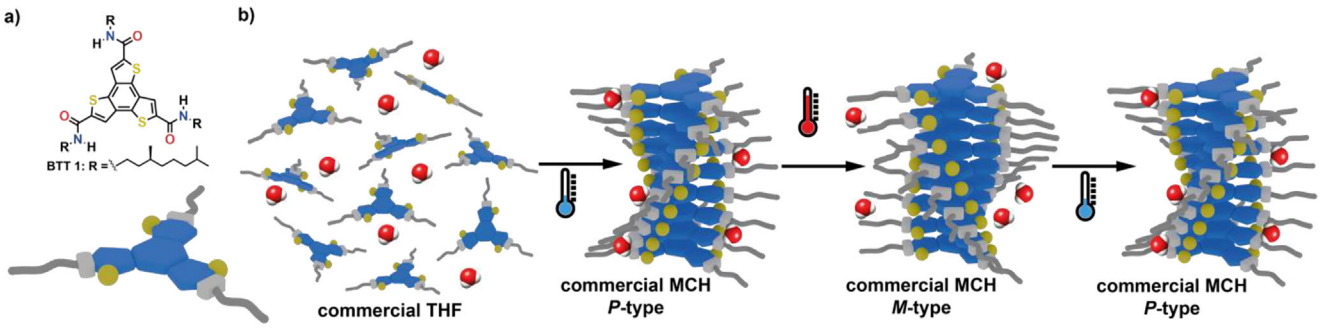

Figure 1. a) Chemical structure of the chiral BTT **1** and illustration of the monomeric species of **1**. b) Schematic illustration of the temperature-dependent stereomutation experienced by the supramolecular polymer formed by BTT **1**, in which water acts as key effector.

functional materials.[22] Noteworthy, in contrast to molecular stereoinversion— which often requires high-energy covalent bond cleavage and formation —the inversion of handedness in chiral supramolecular ensembles can be triggered by external stimuli, owing to the weak and reversible nature of the noncovalent forces governing the formation of the aggregate.[19–21] Common strategies to achieve supramolecular stereomutation include the addition of achiral chemical additives like diazo compounds,[23,24] the formation of cations[25,26] or kinetic traps,[27,28] and, especially, changing the solvent in which the supramolecular polymerization takes place.[29] Directly related to this latter approach, we recently reported the efficient transfer of asymmetry in N-annulated perylenediimides (NPDIs) from the peripheral side chains to the central core. The relative arrangement of the lateral trialkoxyphenyl moieties with respect to the central aromatic core depends on the solvent used for the supramolecular polymer formation. Thus, a single enantiomer of the NPDI can generate columnar aggregates of opposite handedness depending on whether methylcyclohexane (MCH) or toluene (Tol) is utilized to drive the self-assembling process.[29]

In this context, we report herein the synthesis of a new chiral system based on benzotrithiophene (BTT) as the central aromatic core (compound **1** in Figure 1a), which forms helical supramolecular polymers upon self-assembly. The C_3 symmetry of this core allows the system to undergo an unprecedented stereomutation process, in which water acts as an effector, inducing a time-dependent change in the handedness of the resulting helical aggregates (Figure 1b). Our study demonstrates the crucial role of water in this stereoinversion process. Circular dichroism measurements reveal that the presence of a large amount of water in the sample induces a double stereomutation, where the handedness of the aggregates reverses twice, ultimately restoring the initial helicity. In contrast, reducing the water content leads to a single stereomutation process, in which the handedness changes once and remains stable. The duration of this single stereomutation is dependent on the water concentration. These findings raise an intriguing question: does the change in handedness indicate that two helical aggregates with different helicities are in energetic competition? Or, alternatively, is one of them kinetically trapped during synthesis? To elucidate the origins of the stereomutation process in BTT **1** and the influence of water, we have conducted a detailed multi-level computational characterization. The most stable configuration of aggregated **1** features a *syn* arrangement of the BTT moieties, where the sulfur-based cores stack in the same orientation. In this superstructure, we identify two competitive diastereomeric aggregates with different preferred helical orientation. The transition between these self-assemblies involves the rotation of the BTT cores and the amide functional groups. This process is energetically favored by the presence of water molecules via hydrogen bonding with the helical stack. Overall, the results presented herein highlight the significant influence of solvent on the formation of chiral, functional supramolecular polymers, shedding new light on the role of water in modulating stereomutation processes.

Results and Discussion

Synthesis of BTT 1 and Self-Assembling Features in Solution

The synthesis of the benzotrithiophene-based molecule **1** requires the preparation of the previously reported benzo[1,2-b:3,4-b′:5,6-b″]trithiophene-2,5,8-tricarboxylic acid **2**, following the protocol reported by Perepichka and coworkers in 2010.[30] To attain the final amide group in **1**, we have utilized different activating agents like N-ethyl-N′-(3-dimethylaminopropyl)carbodiimide or N,N,N′,N′-tetramethyl-O-(1H-benzotriazol-1-yl)uronium hexafluorophosphate to activate the carboxylic acids, thus favoring the subsequent addition-elimination reaction with (*S*)-3,7-dimethyloctan-1-amine **4**.[31] All these attempts were unfruitful, most probably due to the sparing solubility of the tricarboxylic acid **2**. To solve this drawback, the amide coupling was activated by reacting **2** with pentafluorophenyl trifluoroacetate to afford the triester **3** in good yield. A final amidation reaction of triester **3** with amine **4** yields BTT **1** in good yield (Scheme S1). All the new compounds were characterized by using standard spectroscopic techniques (Supporting Information).

The chemical structure of BTT **1** suggests that this chiral tricarboxamide could form supramolecular polymers by the operation of intermolecular H-bonding interactions between the amide functional groups, reinforced by the π-stacking of the central aromatic core. In fact, the fibrillar nature of the

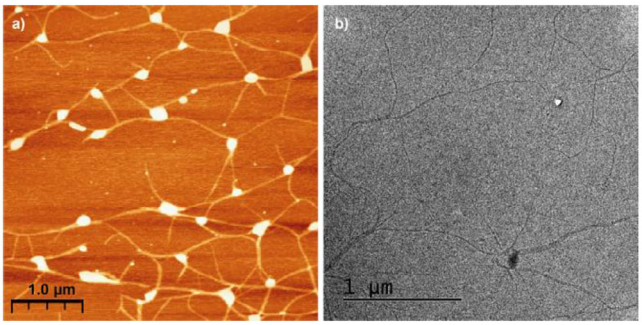

Figure 2. Height AFM a) and TEM b) images of the supramolecular polymers formed by BTT **1** in MCH onto mica (a) and onto a carbon-coated Cu grid (b) as surface ($c_T = 10$ µM).

supramolecular polymers formed by BTT **1** in MCH has been visualized by atomic force microscopy (AFM) and transmission electron microscopy (TEM) imaging. The AFM images of the supramolecular polymers formed upon deposition onto mica as surface show a network of interconnected fibers with typical heights of ~3 nm (Figures 2a and S1a,b). TEM images, registered upon depositing the MCH solution of **1** onto a carbon-coated Cu grid, also show the same fibrillar nature of the supramolecular polymers formed by **1** (Figures 2b and S1c).

To further investigate the aggregation features of BTT **1** and elucidate the noncovalent forces participating in its self-assembly, we tried to carry out common studies like registering ^{1}H NMR spectra in $CDCl_3$ at different concentrations or FTIR spectra in different solvents. Unfortunately, the scarce solubility of the target BTT **1** in pristine chloroform at total concentration (c_T) above 1 mM impedes the registration of these spectra. However, the high solubility of BTT **1** in THF allowed us to prepare a film suitable for registering the FTIR spectrum (Figure S2). The spectrum clearly shows a single N─H stretching band at 3241 cm^{-1} and an Amide I band at 1623 cm^{-1}, diagnostic of the formation of intermolecular H-bonding interactions between the amide functional groups.[32–35] To further evaluate the π-stacking of the aromatic cores, we attempted to register the UV–vis spectrum in different solvents. In chloroform, a good solvent that usually promotes the disassembly of aggregated species,[36] the UV–vis spectrum of **1** at $c_T = 25$ µM displays a broad band centered at 294 nm with a shoulder at 320 nm (Figure 3a). This absorption pattern coincides with that previously reported for monomeric species of referable BTT congeners.[37,38] Due to the limited solubility of BTT **1** in pristine MCH, we prepared a stock solution of **1** in commercial THF at $c_T = 1$ mM. The required volume of this THF solution was added and then dried. Commercial MCH was then added to the residue to achieve a final concentration of 25 µM. The UV–vis spectrum of this MCH solution of **1** shows a clear hypsochromic and hypochromic effect, with an absorption maximum peaking at 273 nm, characteristic of the formation of H-type aggregates (Figure 3a).[39–41] Due to the presence of the stereogenic centers at the peripheral side chains (Figure 1a), the formation of a triple array of H-bonds between the amide functional groups of neighboring C_3-symmetric BTTs could favor an efficient transfer of asymmetry, as occurs in C_3-symmetric tricarboxamides.[42–44] In fact, the CD spectrum of the above-mentioned MCH solution of **1** presents a clear +/− bisignated Cotton effect with maxima at 279 and 261 nm and a zero-crossing point at 273 nm, coincident with the absorption maximum and diagnostic of the formation of *P*-type helical aggregates (Figure 3b).[42–44]

To elucidate the mechanism and derive the corresponding thermodynamic parameters associated with the helical, supramolecular polymerization of **1**, we registered the CD spectra at different temperatures. Heating up the MCH solution of **1** at 90 °C does not yield a complete disassembly of the helical arrangement, as demonstrated by the absorption pattern with the maximum at $\lambda = 273$ nm and, very especially, the identical dichroic pattern to that registered for **1** at 20 °C (Figure 3b). More surprisingly, the CD sign is reverted upon heating up the solution to 90 °C for 5 min (Figure 3b). This temperature-dependent stereomutation could be justified by considering a linear dichroism (LD) effect that contaminates the CD response.[45–47] However, the LD spectra of these samples show a negligible signal, and, therefore, this contamination can be ruled out (Figure S3). To investigate the evolution of the dichroic response after heating the sample for 5 min, we monitored the kinetic behavior of the dichroic signal at 90 °C. As shown in Figure 3c,d, the CD response gradually increases until reaching a plateau at approximately 50 min. Once the dichroic response was stabilized, we cooled the sample down to 20 °C. This heating/cooling (h/c) cycle induces a temporary increase in the CD signal upon reaching 20 °C, followed by a gradual decrease over time. Notably, the dichroic signal vanishes after 135 min and, subsequently, undergoes a sign inversion, ultimately returning to its initial value at 160 min (Figure 3c,d).

Considering the protocol followed to prepare the solution of BTT **1** in MCH, which requires the initial use of the highly hygroscopic THF as solvent, and the relevant role that water molecules can play in the helical organization of supramolecular polymers,[14] we investigated the influence of the water content in the kinetically controlled stereomutation observed in the previous studies. To bias the content of water in the MCH solution of **1**, we prepared dry THF by refluxing this solvent in the presence of sodium and benzophenone. Once the THF was dried, we followed a similar protocol to that described previously to prepare the MCH solution of **1**, and registered the corresponding CD spectra. The CD spectra of the freshly prepared solution of **1** from dry THF and MCH shows the +/− bisignated Cotton effect characteristic of the formation of right-handed helical aggregates (Figure 4a). Despite the handedness of these helical aggregates being identical to that registered for the solutions prepared from commercial THF, the intensity of the dichroic signal is fourfold (compare Figures 3b and 4a). Once again, heating up this solution promotes the inversion of the dichroic response, diagnostic of the formation of left-handed helices (Figures 4a,b). The −/+ dichroic response obtained at 90 °C gradually increases at this temperature until reaching a maximum value at 135 min. Unexpectedly, cooling down the sample at 20 °C slightly increases the intensity of the CD signal, but this increase is not accompanied by a

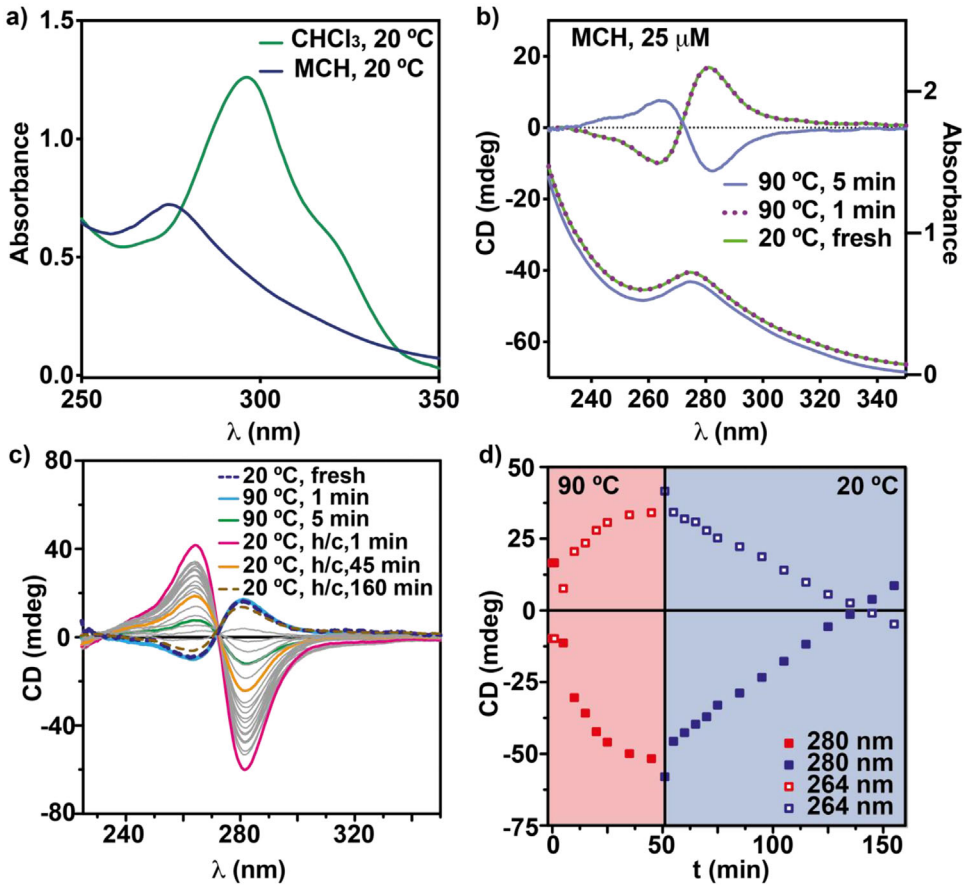

Figure 3. a) UV–vis spectra of BTT **1** in $CHCl_3$ (green) and MCH (blue, $c_T = 25$ μM). b) UV–vis (bottom) and CD (top) spectra of BTT **1** in MCH ($c_T = 25$ μM) at different temperatures. c) CD spectra of BTT **1** in MCH ($c_T = 25$ μM) at different temperatures and times. d) Plot of the variation of the dichroic signal at $\lambda = 280$ (filled squares) and 264 nm (open squares) at 90 (red squares) and 20 °C (blue squares) and at different times. The first point in panel in (d) corresponds to the initial CD measurement at 20 °C, the next one corresponds to the CD measurement at 90 °C and upon 1 min. The red part of the panel depicts the variation of the dichroic response at 90 °C versus time and the blue part shows the variation of the dichroic response at 20 °C, after heating the sample at 90 °C, versus time. ($c_T = 25$ μM; h/c = heating/cooling cycle).

second stereomutation, as occurs in the solution prepared from commercial THF. Therefore, the dichroic response remains stable for long periods of time (Figures 4a,b). To further support the influence of the water content in the stereomutation of the helical aggregates formed by the self-assembly of **1** in MCH, we prepared a new sample by using dry THF and commercial MCH, to which 35 ppm of water were also added. The CD pattern of the freshly prepared solution at 20 °C also presents the +/− bisignated Cotton effect that is inverted upon heating up the solution at 90 °C (Figure 4c,d). The resulting −/+ signal gradually increases, reaching its maximum intensity after 100 min. Cooling down the sample to 20 °C results in a slight increase of the dichroic intensity that remains unaltered for a long period of time (Figure 4c,d).

Importantly, the stereomutation effect observed in MCH implies that the helical supramolecular polymers formed by the self-assembly of **1** are not completely disassembled upon increasing the temperature to 90 °C, as demonstrated by the absorption pattern registered for all the experiments performed in this solvent (Figures 3b and S4). To achieve a complete disassembly of the helical aggregates formed by BTT **1**, we employed decalin as solvent. To prepare this solution, we followed the same protocol as that described for MCH, in which a solution of **1** in dry THF is initially used. The CD spectrum of a freshly prepared solution of **1** in decalin shows the characteristic +/− bisignated Cotton effect, diagnostic of the formation of *P*-type helical aggregates (Figure S5a). Unlike the previous results in MCH, heating this solution to 110 °C completely cancels the dichroic response, indicative of the complete disassembly of the aggregated species. The complete disassembly is also confirmed by the absorption pattern, which shows a broad band peaking at 290 nm, as observed in chloroform (Figure S5a). Noteworthy, cooling down the decalin solution to 20 °C recovers the +/− pattern of the dichroic bands observed in the freshly prepared solution with no sign of stereomutation. However, and despite the lack of stereomutation, a clear increase in the intensity of the dichroic response is observed (Figure S5a). Plotting the variation of the dichroic response versus the temperature yields a non-sigmoidal curve typical of a cooperative mechanism that, in addition, can be fitted to the one-component equilibrium (EQ) model to obtain values for the enthalpy of elongation ($\Delta H_e = -63.1 \pm 1$ kJ mol^{-1}),

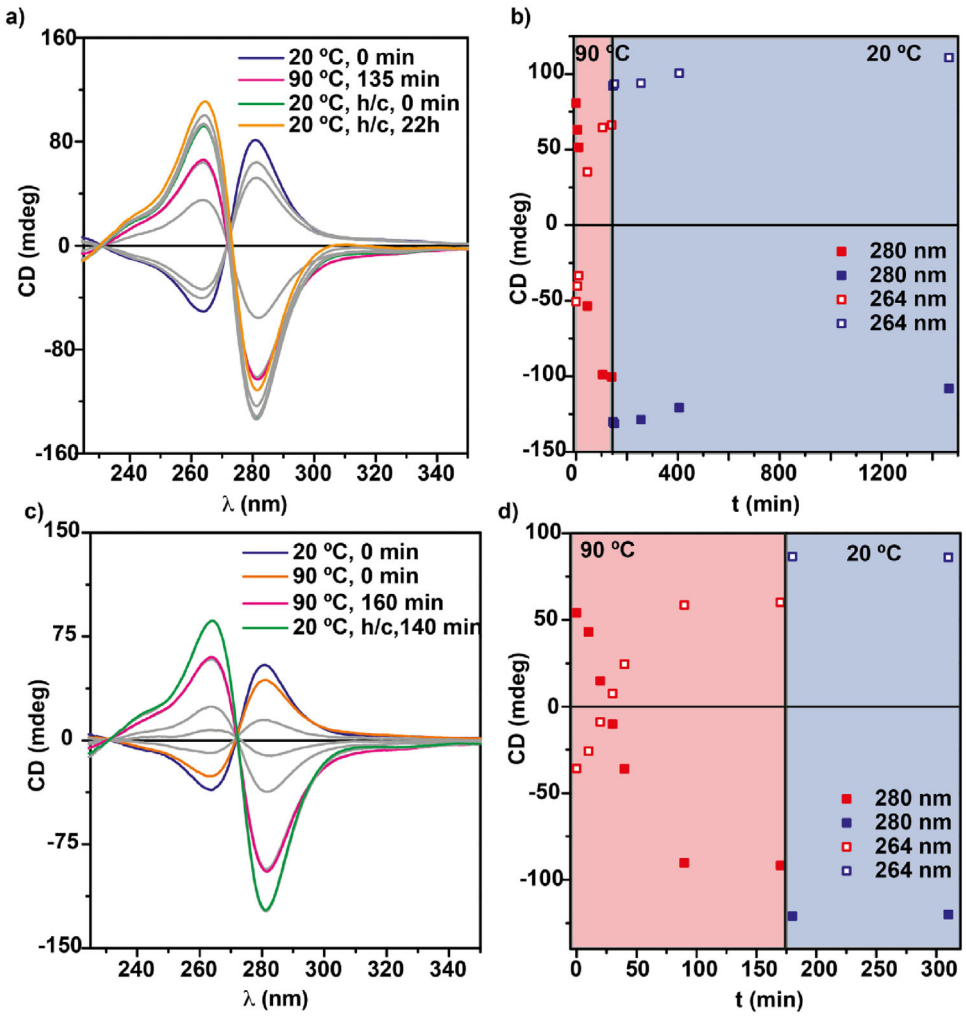

Figure 4. a) CD spectra of BTT **1** at different temperatures and times prepared from dry THF and adding commercial MCH ($c_T = 25$ μM). b) Plot of the variation of the dichroic signal at λ = 280 (filled squares) and 264 nm (open squares) at 90 (red squares) and 20 °C (blue squares) and at different temperatures and times. c) CD spectra of BTT **1** at different temperatures and times prepared from dry THF and adding commercial MCH and 35 ppm of water. d) Plot of the variation of the dichroic signal at λ = 280 (filled squares) and 264 nm (open squares) at 90 (red squares) and 20 °C (blue squares) and at different times. The first point in panels (b) and (d) corresponds to the initial CD measurement at 20 °C, the next one corresponds to the CD measurement at 90 °C and upon 1 min. The red parts of panels (b) and (d) depict the variation of the dichroic response at 90 °C versus time, and the blue parts show the variation of the dichroic response at 20 °C, upon heating the sample at 90 °C, versus time ($c_T = 25$ μM).

enthalpy of nucleation ($\Delta H_n = -25.0 \pm 2$ kJ mol^{-1}), and entropy ($\Delta S = 74.4 \pm 3$ J K^{-1} mol^{-1}) (Figure S5b).[48]

Theoretical Calculations

The unprecedented chiroptical features of BTT **1** prompted us to analyze and understand the supramolecular polymerization and chiral features of the BTT-based building block by developing a set of theoretical calculations in a multi-level approach. First-principles quantum-chemical calculations were carried out for the monomer and trimer aggregates, whereas molecular mechanics/molecular dynamics (MM/MD) calculations were performed on larger supramolecular aggregates of 10 BTT units including explicit solvent. The first structural feature to consider in the chemical structure of BTT **1** is the relative orientation of the amide groups with respect to the sulfur atoms of the BTT core. Some reports evidence that the oxygen atom of the amide tends to point to the sulfur atom of the thiophene rings, this being the most stable conformation.[49,50] Structural geometry optimization by means of the density functional theory (DFT) approach (B3LYP-D3/6-31G(d,p) level) indicates that the conformer in which the oxygen of one amide group faces the sulfur atom of the thiophene ring (**O** orientation) is only 0.114 kcal mol^{-1} more stable than the structure in which the N–H points to the sulfur (**N** orientation). The inclusion of solvent effects slightly increases this energy difference in favor of the most stable conformer in a few tenths of kcal mol^{-1} (Table S1). Note that, in the minimum-energy structures, the amide group is not fully coplanar with the BTT aromatic core in order to minimize steric hindrance (θ angle between 5° and 10°, Figures 5 and

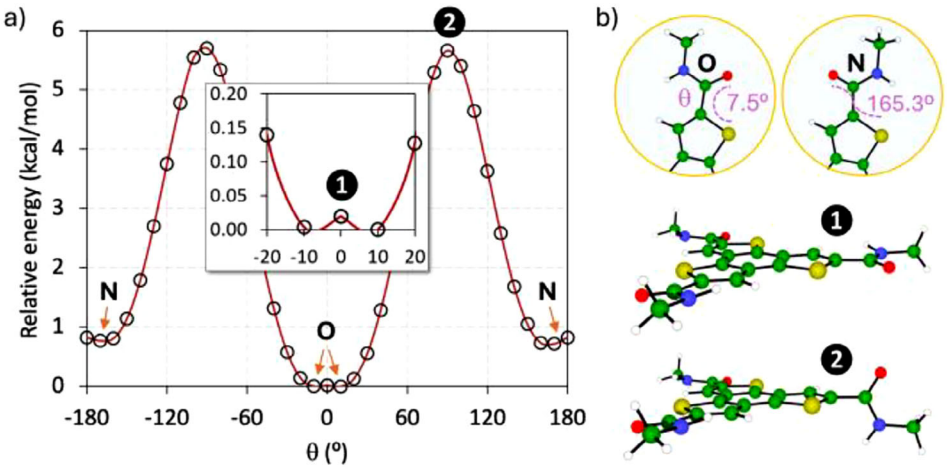

Figure 5. a) θ Dihedral angle scan for the amide orientation with respect to the BTT core. Inset zooming the $\theta = 0°$ region is displayed. b) Representation of the amide orientation in optimized **O** and **N** conformers (top) and transition states connecting the minimum-energy structures **O**(up)/**O**(down) (❶; $\theta = 0°$) and **O**/**N** (❷; $\theta = 90°$) (bottom).

S6). The energy penalty for the amide rotation is key to understanding the viability of reverting the orientation of the amide groups regarding the BTT core, with further implications for helical sense interconversion in the supramolecular aggregate. Theoretical calculations at the same level of theory predict a negligible energy barrier for the amide rotation passing through the fully coplanar conformation (0.02 kcal mol^{-1}), whereas a moderate energy penalty of 5.70 kcal mol^{-1} is calculated for the rotation through the perpendicular amide BTT configuration (Figure 5).

The experimental data reveals that C_3-symmetric **1** can form helical, supramolecular polymers by the operation of a triple H-bonding array and the π-stacking of the aromatic backbones. To ascertain the most plausible seed that grows up toward the formation of a supramolecular BTT assembly, different trimeric aggregates were modelled considering these noncovalent interactions, and their structure was optimized at the B3LYP-D3/6-31G(d,p) DFT level (see the Supporting Information for full details). We explored the formation of trimers with the BTT amide units fully oriented as **OOO** or **NNN** and also with combinations of them: **OON** and **ONN** (Figure S7). Additionally, and in contrast to other C_3-symmetric organic building blocks (e.g., benzene tricarboxamides, benzene triphenylamides, etc.),[42–44,51,52] the BTT cores are able to stack either with the same orientation (*syn*) or with alternating orientation (*anti*) (Figure S7a). In agreement with the experiments, the triple array of H-bonding interactions in the modelled trimers prevails, predicted with N─H···O intermolecular distances in the range of 1.85–1.95 Å upon optimization, and with a BTT helical rotation angle (ϕ) of ca. 40°. Regarding the amide orientation in the trimers (*syn* stacking), DFT calculations predict that the trimer **OON** is the most stable conformation, despite having one chain of H-bonds in the less stable orientation **N**. This result coincides with other investigations reporting that an antiparallel dipole arrangement (up–up–down or down–down–up, 2:1) of the amides leads to the smallest macrodipole for the assembly, resulting in the less energetic amide configuration compared to the fully parallel arrangement (3:0).[53] The **OOO** and **ONN** structures are next in energy, being 0.81 and 1.33 kcal mol^{-1} less stable than **OON**, respectively. Finally, the fully oriented **N** trimer (**NNN**) is predicted to be 4.99 kcal mol^{-1} higher in energy than the minimum-energy **OON** trimer (Figure S7b). Regarding the stacking pattern, theoretical calculations indicate that the *anti* configuration (Figure S7c) is, in all cases, less stable than the *syn* growth (Table S2), most probably due to the less efficient π-stacking between the BTT cores. Therefore, from now on, we focus only on the *syn* assemblies for further analysis and discussion.

The experimental observation indicating a helical inversion upon heating and the reversal process upon cooling suggests that there are two competing supramolecular aggregates of opposite helicity: one more stable at low temperatures and the other prevailing at high temperatures. To consider temperature effects, we performed free energy theoretical calculations, obtaining the enthalpic and entropic energy contributions for each trimeric aggregate. Focusing on the *P*-type helix, theoretical calculations predict that the **OON** assembly provides the smallest enthalpy; the **OOO**, **ONN**, and **NNN** conformers standing 0.80, 1.20, and 4.70 kcal mol^{-1} higher in energy, respectively (Table S3). In contrast, the **OOO** assembly shows a slightly more favorable entropic contribution (440.0 cal mol^{-1} K^{-1}) compared with the **NNN** (437.7 cal mol^{-1} K^{-1}), **OON** (437.4 cal mol^{-1} K^{-1}), and **ONN** (436.4 cal mol^{-1} K^{-1}) assemblies. As a result of combining enthalpic and entropic effects, we predict that conformer **OON** is the most stable structure at room temperature, followed in order by conformers **OOO**, **ONN**, and **NNN** (Table S3). Due to the favorable entropic contribution of **OOO**, it is possible to predict the temperature for the stability transition between conformers **OON** and **OOO**. Our calculations indicate a transition temperature of ca. 330 K (57 °C), which nicely fits within the range of temperatures where the CD pattern inversion takes place experimentally (20–90 °C). This change in the diastereomer stability with temperature, if accompanied by a different helical preference

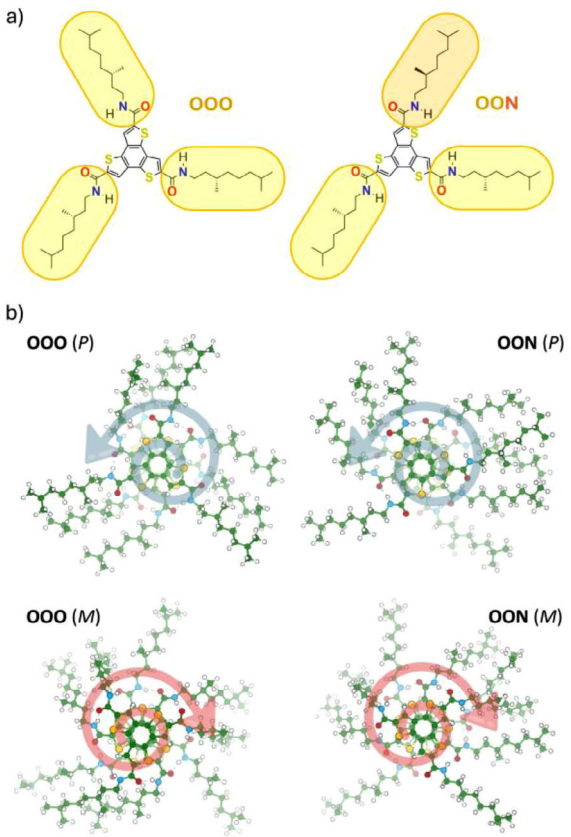

Figure 6. a) Representation of the peripheral chiral aliphatic chain disposition in configurations **OOO** and **OON** for a BTT **1** monomer. b) Minimum-energy structures calculated at the B3LYP-D3/6-31G(d,p) level for trimers **OOO** and **OON**, including the long aliphatic chiral (*S*) chain, in right- (*P*) and left-handed (*M*) helicity. The blue and red curved arrows represent the right- and left-handedness, respectively, of the calculated helical trimers.

for each, could explain the CD sign switching recorded experimentally upon applying the heating/cooling cycle. In fact, related aromatic building blocks have been reported with a similar CD behavior, pointing to a change in the amide orientations (2:1 versus 3:0) as the key factor to explain helical interconversion.[54,55] However, in those works, the authors suggest that the low-temperature assembly is kinetically trapped, whereas, in our case, the thermodynamically stable structure is different as a function of temperature. To give insight into the reason why conformers **OON** and **OOO** prefer different helical senses, we performed DFT calculations including the long aliphatic chains with the stereogenic center (*S*) in the trimeric stack of BTTs. Note that **O** and **N** orientations lead to a different relative disposition of the aliphatic chains when considering the three peripheral branches in 3D space (Figure 6a).

Theoretical calculations at the B3LYP/6-31G(d,p) level indicate that there is barely helical preference in the configuration **OOO**, with the left-handed (*M*) assembly being 0.14 kcal mol^{-1} more stable than the right-handed (*P*)-helix (Figure 6b). Similarly, the *P*- and *M*-helices in the **OON** structure are practically isoenergetic, with the right-handed assembly being 0.36 kcal mol^{-1} more stable than the anticlockwise helix. The large flexibility of the aliphatic chains impedes dissecting the origin of the helical preference upon including the stereogenic center; however, as an achiral solvent is used in the experiments, differences in the chain-to-chain interactions must play a key role. Interestingly, we predict a +/− pattern in the main CD signal for the low-temperature most stable structure **OON** in its preferred helicity (*P*), whereas the high-temperature stabilized **OOO** aggregate in its most stable helicity (*M*) displays a −/+ CD pattern (Figure S8), in good accord with the circular dichroism experiments. This CD signal is demonstrated to originate fully from the helical sense of the π-stacked BTT building blocks, with negligible impact of the amide orientation.

While the thermodynamic landscape of the different minimum-energy structures participating in the process that leads to a change in the CD signal is crucial, the kinetic aspects of such process are also critical to fully rationalize the supramolecular helical inversion. Theoretical calculations at the DFT level were performed in the trimeric assemblies to obtain the transition states required for the handedness flip. First, a change in the helical sense requires a rotation of the BTT building block with respect to its neighbors to efficiently interact through a triple array of well-formed H-bonds. In this regard, two possible motions allow reaching helical inversion (Figure S9): *i*) rotation of the BTT against the helical sense of the aggregate growth passing through an eclipsed transition state (TS) configuration (helical rotation angle $\phi = 0$; eclipsed TS), or *ii*) rotation of the BTT in the same helical sense as the aggregate growth across a transition state where consecutive BTT units are oriented with a rotation angle ϕ of 60° (alternated TS). Our calculations for the **OON** trimer indicate that the alternated transition state is 43.08 kcal mol^{-1} above in energy with respect to the minimum-energy geometry, being 29.28 kcal mol^{-1} more stable than the eclipsed TS. This energy difference is explained by two factors: *i*) the persistence of stabilizing H-bond-like (mostly electrostatic) interactions in the range of 2.5–3.5 Å for the alternated TS, and *ii*) the repulsive S···S contacts in the eclipsed TS, calculated at 3.40 Å (Figure S9). On the other hand, in addition to the BTT core rotation, amide reorientation is required for a correct H-bonding pattern formation in the reversal helicity. Here, we recall the calculations on the energy barrier required for the amide rotation in the BTT monomer (Figure 5), indicating that a transition state through a coplanar conformation is energetically more favorable (barrier of 0.02 kcal mol^{-1}) than the motion through an amide-BTT orthogonal configuration (5.70 kcal mol^{-1}). It is important to note that the rotation across the coplanar TS allows helical inversion but preserves amide conformation (either **O** or **N**). However, and in contrast to building blocks with C_{3v} symmetry, amide rotation through the orthogonal TS switches amide conformation (from **O** to **N** or vice versa, Figure S10). Therefore, reverting the helicity of the BTT aggregate by rotating the amide groups through the orthogonal transition state leads to a diastereomeric conversion, e.g., from **OON** to **NNO** if the three amide groups rotate synchronously. As we predict that helical inversion involves **OOO** and

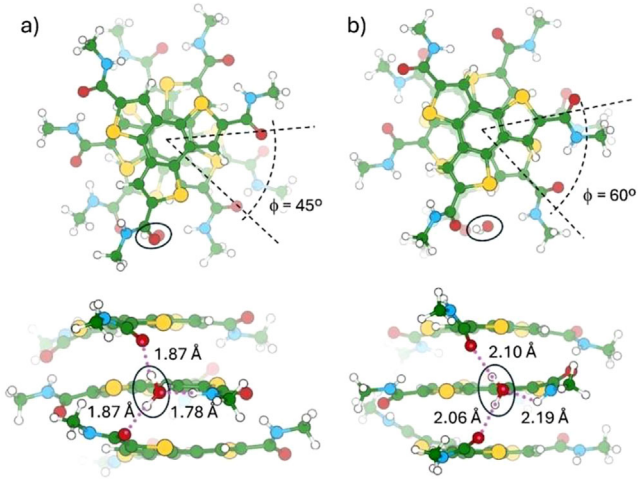

Figure 7. Top and side views of the minimum-energy a) and BTT-alternated transition state b) structures of the **OON** trimer including a water molecule calculated at the B3LYP-D3/6-31G(d,p) level of theory.

OON diastereomers, two out of the three amide groups may undergo rotation through the coplanar TS, which is the energetically favored situation, whereas the third amide is required to rotate across the energetically unfavorable orthogonal TS.

We hypothesize that water molecules present in commercial THF are relevant effectors in facilitating helical inversion, as experimentally evidenced by the changes observed in the CD spectra versus temperature using different solvent conditions. The orthogonal amide rotation pathway cannot be reached through an eclipsed BTT–BTT transition state, so we assume that a BTT rotation through a $\phi = 60°$ alternated disposition with respect to its neighboring units must take place, which is in fact the most stable TS. Theoretical calculations at the B3LYP/6-31G(d,p) level were first performed in an exploratory fashion to unveil how a water molecule interacts with the helical arrangement of the **OON** trimer. We found that the lowest-energy configuration is that in which water favorably interacts through the three amides of consecutive BTT units by means of short H-bonding contacts predicted at 1.87, 1.87, and 1.78 Å (Figure 7a). This leads to a stabilizing structure with an increase in the rotation angle (ϕ) from *ca.* 40° to 45°, thus approaching the BTT-alternated transition state ($\phi = 60°$). We therefore took that water configuration to quantify its impact on the alternated transition state. DFT calculations predict efficient interaction between water and the BTT-alternated TS, with three H-bonds calculated at intermolecular distances of 2.06, 2.10, and 2.19 Å (Figure 7b). As a result, an energy barrier of 21.60 kcal mol^{-1} is obtained for the BTT rotational motion, representing a stabilization of 21.48 kcal mol^{-1} compared to the case without water, and thereby highlighting the key role of water in enhancing the kinetics of helical inversion.

Finally, oligomers of 10 BTT **1** units in the most stable 2:1 (**OON**) and 3:0 (**OOO**) amide configurations were modeled to perform MM/MD calculations and unveil the thermodynamic effect of solvation and the kinetic effect upon water inclusion (see the Supporting Information for full computational details). MM/MD simulations using the NPT ensemble carried out during 0.5 μs at 20 °C and 1 atm pressure indicate that the BTT **1** stacking governed by the triple array of H-bonds becomes progressively more unstable upon increasing solvent polarity from methylcyclohexane to tetrahydrofuran (Figure S11). Our calculations at the MM/MD level are unable to predict helical inversion in the simulated time frame, either at low (20 °C) or at high (90 °C) temperatures, as the process experimentally occurs in the timescale of minutes to hours. Unfortunately, MM/MD level of theory is not accurate enough to predict statistically different relative stability for the two helicities of **OON** at 20 °C ($(1 \pm 40) \times 10^{-4}$ kcal mol^{-1} atom^{-1} in favor of the *P*-helix) or **OOO** at 90 °C ($(1 \pm 30) \times 10^{-4}$ kcal mol^{-1} atom^{-1} in favor of the *M*-helix). Otherwise, we incorporated some water molecules randomly soaked in the solvent box. Theoretical MD calculations predict that water molecules have strong affinity to effectively interact with the amide groups of the BTT **1** assembly (Figure S12). As expected, this affinity is reduced upon increasing temperature, where water molecules detach more easily at 90 °C (Figure S12); however, the interaction between water and BTT **1** still occurs throughout the dynamics. According to the DFT and MM/MD calculations, the presence of water in the solvent is evidenced as essential to facilitate helical inversion by reducing the energy penalty of BTT rotational motion through effective H-bonding interactions with the BTT **1** self-assembly.

Conclusion

In this work, we report the synthesis of the chiral benzotrithiophene BTT **1**, which forms helical supramolecular polymers upon self-assembly. The C_3-symmetric system undergoes an unprecedented temperature-dependent stereomutation process, in which water acts as an effector. CD measurements reveal that the presence of a large amount of water in the sample induces a double temperature-dependent stereomutation, where the handedness of the aggregates reverses twice, ultimately restoring the initial helicity. In contrast, reducing the water content leads to a single stereomutation, in which the handedness changes once and remains stable. The duration of this single stereomutation depends on the water content. To elucidate the origins of the stereomutation in BTT **1** and the influence of water in this process, we have conducted a detailed multi-level computational study. The most stable configuration of aggregated **1** features a *syn* arrangement of the BTT moieties where the sulfur-based cores stack in the same orientation. In this superstructure, two competitive diastereomeric aggregates with different preferred helicity are identified as a result of the relative amide orientation with respect to the BTT core. The transition between these self-assemblies involves the rotation of the BTT cores and the amide functional groups. Our theoretical calculations reveal that this process is strongly favored in the presence of water molecules through effective hydrogen-bonding with the BTT **1** self-assembly. Overall, the results presented herein demonstrate the significant influence of water, even in traces,

present in the solvent on the formation of chiral functional supramolecular polymers, shedding new light on the role of water in modulating self-assembly and stereomutation processes.

Supporting Information

The authors have cited additional references within the Supporting Information.[24,29–38]

Acknowledgements

Financial support by MCIN/AEI/10.13039/501100011033 and the European Union NextGenerationEU/PRTR (PID2023-146971NB-I00, PID2021-128569NB-I00, EIN2020-112276-SUPRAGAPCAT, PID2021-125429NA-I00, CNS2022-135129, María de Maeztu CEX2021-001202-M, and TED2021-131255B-C44) is acknowledged. M.G.I. thanks Santander Talent Attraction Research (STAR2). A.F.-R. acknowledges the Generalitat Valenciana for the CIAPOS/2023/316 grant.

Conflict of Interests

The authors declare no conflict of interest.

Data Availability Statement

The data that support the findings of this study are available from the corresponding author upon reasonable request.

Keywords: Benzotrithiophene · Stereomutation · Supramolecular polymers · Theoretical calculations · Water

[1] Y. Marcus, *Chem. Soc. Rev.* **1993**, *22*, 409. https://doi.org/10.1039/cs9932200409.
[2] P. Ball, *Chem. Rev.*, **2008**, *108*, 74.
[3] K. A. Dill, S. Bromberg, K. Yue, H. S. Chan, K. M. Ftebig, D. P. Yee, P. D. Thomas, *Protein Sci.* **1995**, *4*, 561.
[4] I. Tinoco, C. Bustamante, *J. Mol. Biol.* **1999**, *293*, 271–281. https://doi.org/10.1006/jmbi.1999.3001.
[5] M. F. J. Mabesoone, A. R. A. Palmans, E. W. Meijer, *J. Am. Chem. Soc.* **2020**, *142*, 19781–19798. https://doi.org/10.1021/jacs.0c09293.
[6] E. Krieg, M. M. C. Bastings, P. Besenius, B. Rybtchinski, *Chem. Rev.* **2016**, *116*, 2414.
[7] A. N. Edelbrock, T. D. Clemons, S. M. Chin, J. J. W. Roan, E. P. Bruckner, Z. Álvarez, J. F. Edelbrock, K. S. Wek, S. I. Stupp, *Adv. Sci.* **2021**, *8*, 2004042.
[8] M. H. Bakker, C. C. Lee, E. W. Meijer, P. Y. W. Dankers, L. Albertazzi, *ACS Nano* **2016**, *10*, 1845. https://doi.org/10.1021/acsnano.5b05383.
[9] M. A. Martínez, D. Aranda, E. Ortí, J. Aragó, L. Sánchez, *Org. Chem. Front.* **2023**, *10*, 1959–1967. https://doi.org/10.1039/D3QO00111C.
[10] T. F. A. De Greef, M. M. J. Smulders, M. Wolffs, A. P. H. J. Schenning, R. P. Sijbesma, E. W. Meijer, *Chem. Rev.* **2009**, *109*, 5687–5754. https://doi.org/10.1021/cr900181u.
[11] M. Liu, L. Zhang, T. Wang, *Chem. Rev.* **2015**, *115*, 7304–7397. https://doi.org/10.1021/cr500671p.
[12] F. García, R. Gómez, L. Sánchez, *Chem. Soc. Rev.* **2023**, *52*, 7524.
[13] N. J. Van Zee, B. Adelizzi, M. F. J. Mabesoone, X. Meng, A. Aloi, R. H. Zha, M. Lutz, I. A. W. Filot, A. R. A. Palmans, E. W. Meijer, *Nature* **2018**, *558*, 100–103. https://doi.org/10.1038/s41586-018-0169-0.
[14] *Dynamic Stereochemistry of Chiral Compounds: Principles and Applications*, C. Wolff. Ed., Royal Society of Chemistry, Cambdrige, UK, **2007**.
[15] W.-B. Gao, Z. T. Li Tong, X. Dong, H. Qu, L. Yang, A. C.-H. Sue, Z.-Q. Tian, X.-Y. Cao, *J. Am. Chem. Soc.* **2023**, *145*, 17795–17804. https://doi.org/10.1021/jacs.3c04761.
[16] X. Yuan, Y. Zhang, Y. Li, J. Yin, S. Wang, T. Xiong, Q. Zhang, *Angew. Chem. Int. Ed.* **2023**, *62*, e202313770. https://doi.org/10.1002/anie.202313770.
[17] M. W. Gillick-Healy, E. V. Jennings, H. Müller-Bunz, Y. Ortin, K. Nikitin, D. G. Gilheany, *Chem. - Eur. J.* **2017**, *23*, 2332–2339. https://doi.org/10.1002/chem.201604080.
[18] G. Liu, M. G. Humphrey, C. Zhang, Y. Zhao, *Chem. Soc. Rev.* **2023**, *52*, 4443–4487. https://doi.org/10.1039/D2CS00476C.
[19] B. Shen, Y. Kim, M. Lee, *Adv. Mater.* **2020**, *32*, 1905669. https://doi.org/10.1002/adma.201905669.
[20] L. Zhang, H.-X. Wang,S. Lia, M. Liu, *Chem. Soc. Rev.* **2020**, *49*, 9095–9120. https://doi.org/10.1039/D0CS00191K.
[21] Y. Ai, Y. Zhang, Y. Jiang, G. Zhuang, Y. Li, *Nat. Comm.* **2025**, *16*, 1971. https://doi.org/10.1038/s41467-025-57114-z.
[22] G. Liu, J. Sheng, H. Wu, C. Yang, G. Yang, Y. Li, R. Ganguly, L. Zhu, Y. Zhao, *J. Am. Chem. Soc.* **2018**, *140*, 6467–6473. https://doi.org/10.1021/jacs.8b03309.
[23] H. Choi, S. Heo, S. Lee, K. Y. Kim, J. H. Lim, S. H. Jung, S. S. Lee, H. Miyake, J. Y. Lee, J. H. Jung, *Chem. Sci.* **2020**, *11*, 721–730. https://doi.org/10.1039/C9SC04958D.
[24] S. Arias, F. Freire, E. Quiñoá, R. Riguera, *Polym. Chem.* **2015**, *6*, 4725–4733. https://doi.org/10.1039/C5PY00587F.
[25] J. S. Valera, R. Gómez, L. Sánchez, *Angew. Chem. Int. Ed.* **2019**, *58*, 510–514. https://doi.org/10.1002/anie.201809272.
[26] L. López-Gandul, C. Naranjo, C. Sánchez, R. Rodríguez, R. Gómez, J. Crassous, L. Sánchez, *Chem. Sci.* **2022**, *13*, 11577–11584. https://doi.org/10.1039/D2SC03449B.
[27] C. Kulkarni, P. A. Korevaar, K. K. Bejagam, A. R. A. Palmans, E. W. Meijer, S. J. George, *J. Am. Chem. Soc.* **2017**, *139*, 13867–13875. https://doi.org/10.1021/jacs.7b07639.
[28] J. S. Valera, R. Sánchez-Naya, F. J. Ramírez, J. L. Zafra, R. Gómez, J. Casado, L. Sánchez, *Chem. - Eur. J.* **2017**, *23*, 11141–11146. https://doi.org/10.1002/chem.201702391.
[29] M. S. Martínez, A. Doncel-Giménez, J. Cerdá, J. Calbo, J. Rodríguez, J. Aragó, J. Crassous, E. Ortí, L. Sánchez, *J. Am. Chem. Soc.* **2021**, *143*, 13281–13291. https://doi.org/10.1021/jacs.1c06125.
[30] T. Taerum, O. Lukoyanova, R. Wylie, D. F. Perepichka, *Org. Lett.* **2009**, *11*, 3230–3233. https://doi.org/10.1021/ol901127q.
[31] M. Fontana, H. Chanzy, W. Caseri, P. Smith, A. P. H. J. Schenning, E. W. Meijer, F. Gröhn, *Chem. Mater.* **2002**, *14*, 1730–1735. https://doi.org/10.1021/cm0109793.
[32] M. Wehner, M. I. S. Röhr, M. Bühler, V. Stepanenko, W. Wagner, F. Würthner, *J. Am. Chem. Soc.* **2019**, *141*, 6092–6107. https://doi.org/10.1021/jacs.9b02046.
[33] N. M. Casellas, I. Urbanaviciute, T. D. Cornelissen, J. A. Berrocal, T. Torres, M. Kemerink, M. García-Iglesias, *Chem. Commun.* **2019**, *55*, 8828–8831. https://doi.org/10.1039/C9CC02466B.

[34] S. Ogi, V. Stepanenko, K. Sugiyasu, M. Takeuchi, F. Wurthner, *J. Am. Chem. Soc.* **2015**, *137*, 3300–3307. https://doi.org/10.1021/ja511952c.
[35] L. López-Gandul, A. M. Blanco, F. García, L. Sánchez, *Angew. Chem. Int. Ed.* **2023**, *62*, e202308749, (1 of 9).
[36] P. A. Korevaar, C. Schaefer, T. F. A. De Greef, E. W. Meijer, *J. Am. Chem. Soc.* **2012**, *134*, 13482–13491. https://doi.org/10.1021/ja305512g.
[37] N. M. Casellas, S. Pujals, D. Bochicchio, G. M. Pavan, T. Torres, L. Albertazzi, M. García-Iglesias, *Chem. Commun.* **2018**, *54*, 4112–4115. https://doi.org/10.1039/C8CC01259H.
[38] N. M. Casellas, L. Albertazzi, S. Pujals, T. Torres, M. García-Iglesias, *Chem. - Eur. J.* **2021**, *27*, 11056–11060. https://doi.org/10.1002/chem.202101660.
[39] M. Kasha, *Discuss. Faraday Soc.* **1950**, *9*, 14.
[40] R. M. Hochstrasser, M. Kasha, *Photochem. Photobiol.* **1964**, *3*, 317–331. https://doi.org/10.1111/j.1751-1097.1964.tb08155.x.
[41] F. Würthner, T. E. Kaiser, C. R. Saha-Möller, *Angew. Chem. Int. Ed.* **2011**, *50*, 3376–3410. https://doi.org/10.1002/anie.201002307.
[42] M. M. J. Smulders, A. P. H. J. Schenning, E. W. Meijer, *J. Am. Chem. Soc.* **2008**, *130*, 606–611. https://doi.org/10.1021/ja075987k.
[43] F. García, P. M. Viruela, E. Matesanz, E. Ortí, L. Sánchez, *Chem.–Eur. J.* **2011**, *17*, 7755.
[44] F. García, L. Sánchez, *J. Am. Chem. Soc.* **2012**, *134*, 734.
[45] A. Tsuda, M. D. Alam, T. Harada, T. Yamaguchi, N. Ishii, T. Aida, *Angew. Chem. Int. Ed.* **2007**, *46*, 8198–8202. https://doi.org/10.1002/anie.200703083.
[46] M. Wolffs, S. J. George, Z. Tomovic, S. C. J. Meskers, A. P. H. J. Schenning, E. W. Meijer, *Angew. Chem. Int. Ed.* **2007**, *46*, 8203–8205. https://doi.org/10.1002/anie.200703075.
[47] J. Buendía, J. Calbo, E. Ortí, L. Sánchez, *Small* **2017**, *13*, 1603880.
[48] H. M. M. ten Eikelder, A. J. Markvoort, T. F. S. de Greef, P. A. J. Hilbers, *J. Phys. Chem. B* **2012**, *116*, 5291–5301. https://doi.org/10.1021/jp300622m.
[49] M. Ueda, T. Aoki, T. Akiyama, T. Nakamuro, K. Yamashita, H. Yanagisawa, O. Nureki, M. Kikkawa, E. Nakamura, T. Aida, Y. Itoh, *J. Am. Chem. Soc.* **2021**, *143*, 5121–5126. https://doi.org/10.1021/jacs.1c00823.
[50] S. J. Coles, P. A. Gale, M. B. Hursthouse, M. E. Light, C. N. Warriner, *Supramolecular Chem.* **2004**, *16*, 469.
[51] E. E. Greciano, S. Alsina, G. Ghosh, G. Fernández, L. Sánchez, *Small Methods* **2020**, *4*, 1900715. https://doi.org/10.1002/smtd.201900715.
[52] S. Díaz-Cabrera, Y. Dorca, J. Calbo, J. Aragó, R. Gómez, E. Ortí, L. Sánchez, *Chem. - Eur. J.* **2018**, *24*, 2826–2831. https://doi.org/10.1002/chem.201706070.
[53] K. K. Bejagam, G. Fiorin, M. L. Klein, S. Balasubramanian, *J. Phys. Chem. B* **2014**, *118*, 5218–5228. https://doi.org/10.1021/jp502779z.
[54] B. Adelizzi, I. A. W. Filot, A. R. S. Palmans, E. W. Meijer, *Chem. - Eur. J.* **2017**, *23*, 6103–6110. https://doi.org/10.1002/chem.201603938.
[55] K. K. Bejagam, C. Kulkarni, G. J. Subi, S. Balasubramanian, *Chem. Commun.* **2015**, *51*, 16049–16052. https://doi.org/10.1039/C5CC05569E.

Manuscript received: August 11, 2025
Revised manuscript received: October 06, 2025
Manuscript accepted: October 21, 2025
Version of record online: ■■, ■■